Wet powder spraying – A versatile and highly effective technique for the application of spinel-type protective coatings on SOC interconnects

Michael Wolff¹, Alexander Schwiers¹, Kai Wilkner¹, Doris Sebold¹, Norbert H. Menzler*,¹

¹ Forschungszentrum Jülich GmbH, Institute of Energy and Climate Research, IEK-1: Materials Synthesis and Processing, 52425 Jülich, Germany

* Corresponding author, n.h.menzler@fz-juelich.de

Keywords

Solid oxide cell (SOC), interconnect, protective coating, ceramic processing

Abstract

Chromia-forming metallic interconnects used for solid oxide cells require protective coatings to prevent chromium poisoning of other cell components. This study focuses on Mn_{1.0}Co_{1.9}Fe_{0.1}O₄ -coated Crofer 22 H interconnects fabricated by wet powder spraying, which is a versatile, cost-effective, and scalable coating technique. The investigation and fine-tuning of relevant parameters along the process chain provide a fundamental understanding of their impact on coating quality and thermomechanical stability. The correlation with cross-sectional analysis and area-specific contact resistance (ASR) measurements supports the parameter evaluation. Mid-term thermal testing demonstrates excellent chromium retention, as well as chemical and mechanical stability of the protective layer on real component interconnect substrates. With an ASR below 10 m Ω cm² after 1000 h at 800 °C, wet powder spraying represents a viable alternative to established but more expensive processes.

1. Introduction

Solid oxide cells (SOCs) are fuel-flexible energy conversion devices that provide high efficiency and environmental friendliness, making them a promising alternative to traditional energy-conversion systems. In the early stages of SOC development, operation temperatures of 900–1000 °C and ceramic interconnects were required. The need to lower operating temperatures to reduce costs and improve long-term stability has led to the exploration of metallic interconnects as more economically viable and mechanically robust alternatives [1], especially for planar designs. Ferritic stainless

steels with high chromium concentrations, such as Crofer 22 APU/H and AISI 441, are particularly promising for fuel-electrode-supported cells due to their excellent oxidation resistance and compatible coefficients of thermal expansion (CTE) [2–4]. Despite their composition-tailored development, untreated interconnects are still not sufficiently stable for long-term operation in commercial applications. Cr₂O₃ scale formation on the steel surface during operation in O₂/H₂O leads to a sequence of different degradation mechanisms which impacts on the whole cell performance:

- (1) A decrease in electrical conductivity and, thus, an increase in the contact area specific resistance (ASR)
- (2) Cr₂O₃ reacts with oxygen and water vapor, forming volatile CrO₂(OH)₂ and CrO₃, respectively [5]
- (3) These volatile and highly toxic compounds migrate into the air electrode, leading to the formation of unwanted and electrochemically inactive side products depending on the electrode material

Even double-layer oxide-forming steels like Crofer 22 APU/H (inner chromia and outer Cr-Mn-spinel layer) evaporate too much Cr species for envisaged real-world long-term applications (>50,000 h). The evaporation "pressure" above a layer depends on the source (layer chemistry and microstructure) and the sink (atmospheric conditions incl. temperature, oxidizing/reducing environment, etc.). Above Cr-Mn-spinel, the Cr partial pressure is lower than chromia, thus the interconnect evaporates less Cr species [6].

Protective layer coatings have proven to be highly effective in improving Cr retention of the interconnects and thus improving the overall stack performance. So far, a variety of different material compositions and coating techniques has been explored [7,8]. Most of the studied coatings either belong to the spinel or perovskite group. For instance, lanthanum chromite (LaCrO₃) has not only seen application as an interconnect material, but also as a coating material for steel interconnects [9–11]. Although perovskite-based coatings show great electrical conductivity and high temperature stability under oxidizing conditions, their ability to suppress chromium evaporation is limited [12]. In recent years, Mn-Co and Mn-Cu-based spinels have become more popular due to their excellent electrical conductivity, thermal expansion match, high-temperature stability, and improved chromium retention functionality [13–17]. Physical vapor deposition (PVD), electrophoretic deposition (EPD), screen printing (SP), and atmospheric plasma spray (APS) are noteworthy techniques for the application of interconnect coatings with mid- to long-term stability [18–21].

Despite great performance and scientific value, the approach that has the potential for scale-up and industrial application has yet to be identified. The wet powder spraying (WPS) technique originates from in-house feasibility studies conducted more than 20 years ago and has been further developed over the past few years [22,23]. The main principle is straight-forward. A ceramic slurry is sprayed onto a substrate using an automated spraying gun and a carrier gas, enabling the coating of small planar or tubular substrates as well as real-shaped components within a few seconds. Organic slurry additives are burned out and the coating layer is densified by a follow-up thermal treatment. This gives rise to significant benefits regarding processing speed in contrast to alternative coating techniques, such as PVD or APS. By contrast, thermomechanical stress on the thin metallic substrate is not an issue for WPS processing which is

conducted at room temperature. If all coating, de-bindering, and heat treatment steps are developed carefully, the final heat treatment could be integrated into the start-up procedure of stacks, thereby omitting a prior additional heating step.

In this study, WPS is utilized to apply protective coatings of Mn_{1.0}Co_{1.9}Fe_{0.1}O₄ (MCF) on Crofer 22 H. The aim of the present work is to develop a fundamental process understanding by examining the correlation between WPS processing and post-processing parameters with microstructure, coating quality, and ASR. For this purpose, different parameter sets are evaluated via scanning electron microscopy (SEM), energy dispersive X-ray spectroscopy (EDS), and white light interferometry. ASR data of coated and uncoated interconnect substrates derived by the 4-probe technique are used for quality assessment. Finally, the adaption to a real component interconnect and thermal mid-term studies will provide an answer to the question: Can wet powder spraying for SOC interconnects accomplish both efficiency and competitive performance?

2. Experimental

In the present study, the ferritic steel Crofer 22 H (VDM Metals, Germany) with a thickness of 0.5 mm and a coupon size of 20 x 20 mm² was used as a first substrate material [24]. Mid-term testing was performed on pre-cut sheets from a channel-type interconnect. Coatings were applied by wet powder spraying of a MCF suspension. Suspensions with a solid content of about 38wt% were prepared by dispersing commercially available MCF powder (KCeracell, Republic of Korea) in a solvent based on ethanol with suitable amounts of dispersant, binder, and defoaming agent to enhance the processability. Particles in the suspension showed a monomodal particle size distribution with d₁₀=0,6 μm, d₅₀=0.8 μm and d₉₀=1.0 μm. Coating application was performed using a large-scale wet powder spraying device with an automated spraying gun (built in-house). The coating sequence was programmed in terms of sprayer head movement speed and position in x- and y-direction. After the final layer application, substrates were dried in ambient air conditions. Thermal treatment was conducted in a two-step process in a chamber furnace. At sintering temperatures between 800 °C and 1000 °C and holding times between 2 h and 100 h, samples were first reduced in an Ar/ 3 % H₂ atmosphere followed by re-oxidization in ambient air. Mid-term thermal treatment studies were performed with holding times of 500 h or 1000 h, respectively.

Microstructural analysis was performed on the cross section of polished samples by scanning electron microscopy (SEM) with energy dispersive X-ray spectroscopy (EDS). Measurements were either performed with a tabletop scanning electron microscope (TM3030, Hitachi High Technology, Japan) or a Zeiss Ultra 55 SEM (Carl Zeiss NTS GmbH, Germany) equipped with an EDS system Oxford X-Max 80 mm² (Oxford Instruments, Germany). The porosity of SEM cross-sections was determined by digital image analysis using Fiji/ImageJ (Ver. 1.53k, Wayne Rasband and contributors, National Institutes of Health, USA). Comparable sections of the individual SEM images were selected for e.g. porosity calculations to provide comparability; surface regions and interface regions were ruled out. Sample topography and

roughness were investigated by optical profilometry (Cyber Scan CT350T, Cyber Technologies, Germany).

Area-specific resistance measurements were performed in a chamber furnace in air at 800 °C. Coated and uncoated interconnect specimens of 1 x 1 cm² were contacted to an La_{0.58}Sr_{0.4}Co_{0.2}Fe_{0.8}O_{3-x} (LSCF) pellet with Pt paste. The sample was positioned between two platinum mesh electrodes and pressed together during the measurement with a surface weight of 1.5 kg cm⁻² (Figure 1). Voltage measurements were performed with a Fluke 289 digital multimeter with a typical current density of 0.5 A cm⁻². To compensate for device- and sample-related deviations, mean ASR values and standard deviations were calculated by measuring three identically processed specimens for each sample type.

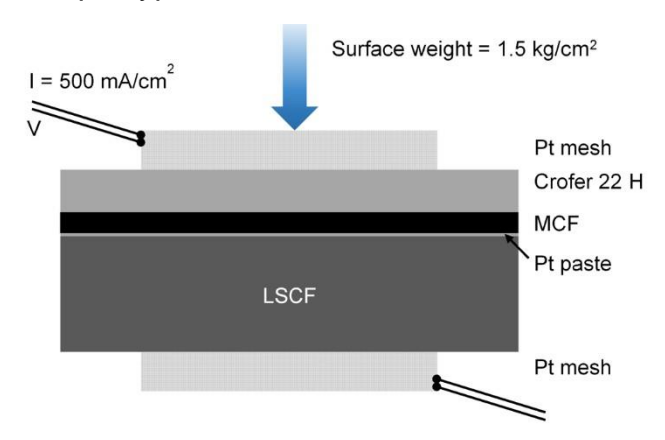


Figure 1: Schematic representation of the ASR test setup. The pre-sintered and polished LSCF electrode is pressed against the coated interconnect steel with Pt paste during measurement at 800 °C.

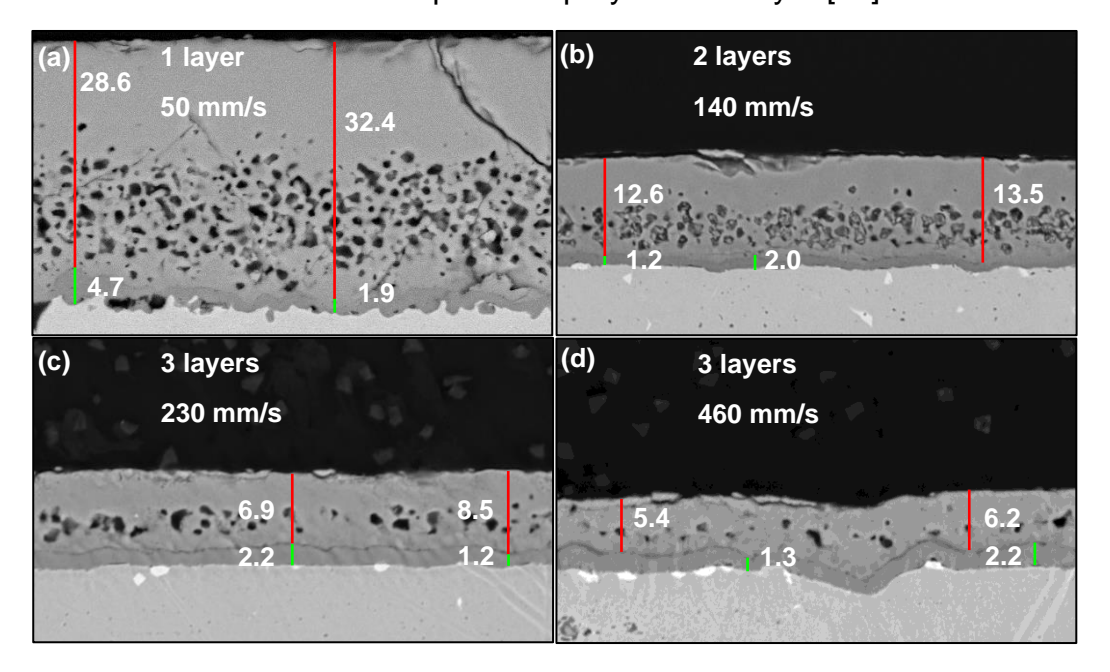
3. Results and discussion

3.1 Processing of protective barrier coatings

In general, a wide range of process parameters must be considered for the WPS process development and optimization: spraying speed, nozzle size, distance between sprayer head and substrate, gas pressure, number of layers, and drying time between the respective coating steps. Preliminary studies revealed a varying impact of these parameters on the overall coating result. (Certain parameter pairs have shown cross-interplay, e.g., gas pressure and coating speed or sprayer head distance and coating speed.) Furthermore, surface pre-treatment, slurry composition, and post-sintering must also be taken into account. Although a design of experiments may offer certain advantages for process optimization, a semi-empirical approach was preferred due to the quantity of co-dependent process variables. Herein, each process variable was evaluated alone while keeping all other variables constant along the process chain. Based on post-analysis results, the parameter was then either further refined or set as a constant for further coating experiments. Following this routine, the spraying distance, nozzle size, gas pressure, and drying time were refined prior to the actual coating studies, providing satisfactory and reproduceable results.

The number of layers and the coating speed as remaining key variables were further explored in detail to improve efficiency and controllability of the WPS process. Two main findings resulted from SEM cross-sectional image analysis (Figure 2). First, the

number of applied coating layers correlated linearly with the coating thickness under the premise that the coating speed remained constant. This finding was revealed by measuring the coating thickness in cross-sectional SEM images after sintering. With a coating speed of 230 mm s⁻¹, three coating layers yielded a thickness of 9.4 µm, four layers 12.1 µm, and seven 20.7 µm, for instance. Hence, all samples showed a thickness per layer of ~3.0 µm. Second, the layer thickness decreased with the coating speed exponentially. As a consequence, coating speeds below 100 mm s⁻¹ led to high coating thicknesses, exceeding reasonable values needed for the chromium barrier functionality. Since values above 250 mm s⁻¹ only showed a minor impact on coating thickness, 140–230 mm s⁻¹ can be considered the optimal coating speed range. Overall, coating thickness can be fine-tuned more conveniently by adjusting the number of layers. It should be noted that no "ideal" coating thickness exists. The coating must have a minimum thickness to cover all interconnect areas, including edges and flanks, but it should not be too thick as this would increase the overall ohmic resistance in the repeat unit. Another aspect is the Cr diffusivity within the layer. If the layer is gas-tight, diffusion can only take place via solid-state diffusion. The preliminary work of Grünwald et al. and long-term tests showed that Cr diffusivity within plasmasprayed MCF is quite low. Even after 10,000 h of annealing time, no detectable amounts of Cr could be found in a plasma-sprayed MCF layer [25].



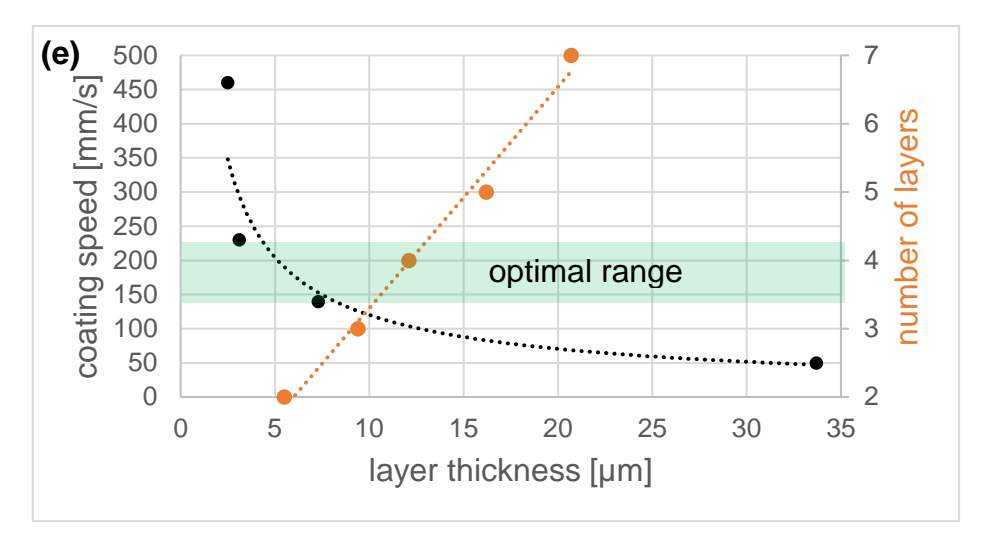


Figure 2: (a - d) Electron micrographs of polished cross sections of Crofer 2 H/MCF processed with different coating speeds and number of layers. (e) Correlation diagram showing the impact of parameter variation on the resulting layer thickness. The orange line shows the layer thickness as a function of the number of layers, whereas the black line shows the layer thickness depending on the coating speed.

3.2 Microstructure

Regardless of process parameters, WPS-derived protective coatings have shown comparable cross-sectional structures: an interlayer at the interface to the substrate, followed by MCF with closed porosity in the middle area, and finally a dense area of MCF in the top region (Figure 3). Preliminary WPS studies showed that the porosity of the MCF layer can be considerably reduced by increasing the drying time between the respective coating steps, indicating the high porosity of thicker coatings could partly be to solvent evaporation effects. A certain porous character remained, nevertheless. This finding is consistent with previous studies on spinel-based interconnect coatings derived by wet-chemical (slurry coating, electrophoresis, screen-printing) as well as dry-chemical (physical vapor deposition, plasma spraying) coating techniques [26–28].

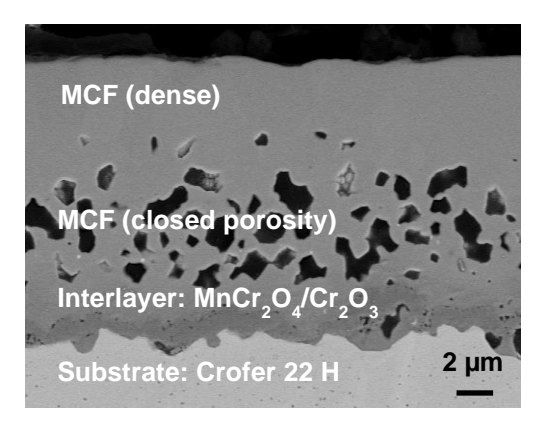


Figure 3: SEM cross showing the typical microstructure section of MCF-coated Crofer 22 H

Distinct differences were observed regarding crack and pore formation tendency as well as interlayer microstructure (Figure 2 a–d). At a coating speed of 140 m s⁻¹, a more diffuse interlayer between MCF and Crofer 22 H with a thickness ranging between 1.9 µm and 4.7 µm was observed. Furthermore, an enlarged area with closed porosity

as well as several large cracks had formed. Even though these cracks did not propagate through the whole coating layer, they may have detrimental effects on the chromium evaporation rate in long-term application. Coating layers derived with speeds between 140 mm s⁻¹ and 460 mm s⁻¹ were continuous without cracks or defects, and the pore formation tendency slightly decreased with decreasing coating thickness. The interlayers showed less thickness variation with comparable values in the range of 1.2–2.0 µm. According to previous studies, this interlayer either consists of Cr₂O₃, Mn_xCr_yO₄ or a mixture of both[29]. In any case, the interlayer exhibits electric conductivities 3–4 orders of magnitude lower than MCF [8]. (The composition of the interlayer will be further addressed in 3.5). EDS analysis has shown that Cr migration is not an issue for MCF layers with closed porosity [25]. Based on these findings, an impact on interlayer scale thickness, however, is expected. It is therefore of great importance to include the interlayer thickness process during parameter assessment. (This topic will be further discussed in section 3.4.)

3.3 Coating layer thickness

This section aims to identify the optimal coating thickness based on ASR measurements. Neither very thin nor thick coatings are desirable for different reasons: Thinner coatings are prone to be consumed by reaction with the chromia scale or they may not be able to cover rough-structured oxide scales completely [30]. Furthermore, coating defects and pores become more critical for low coating thicknesses and can lead to unhindered Cr evaporation. Increased mechanical stability and longevity of thicker MCF coatings give rise to economic, ecological, and ethical disadvantages due to the high cobalt content of MCF.

As discussed in Section 3.1, thick single-layer coatings derived at low coating speeds tended to form cracks and an increased number of closed pores. This raised the following question: can this issue be tackled by applying multiple thinner coating layers instead, providing more time for particle arrangement and slow, controlled solvent evaporation in the green body? To address this question, samples with a different number of coating layers were prepared and ASR measurements were carried out and compared to bare Crofer 22 H substrates. Samples with one, three, five, and seven layers (applied with a coating speed of 230mm/s each) of MCF were tested after 24 h (L1a–L7a) and after thermal treatment for 500 h at 800 °C (L1b–L7b) in each case.

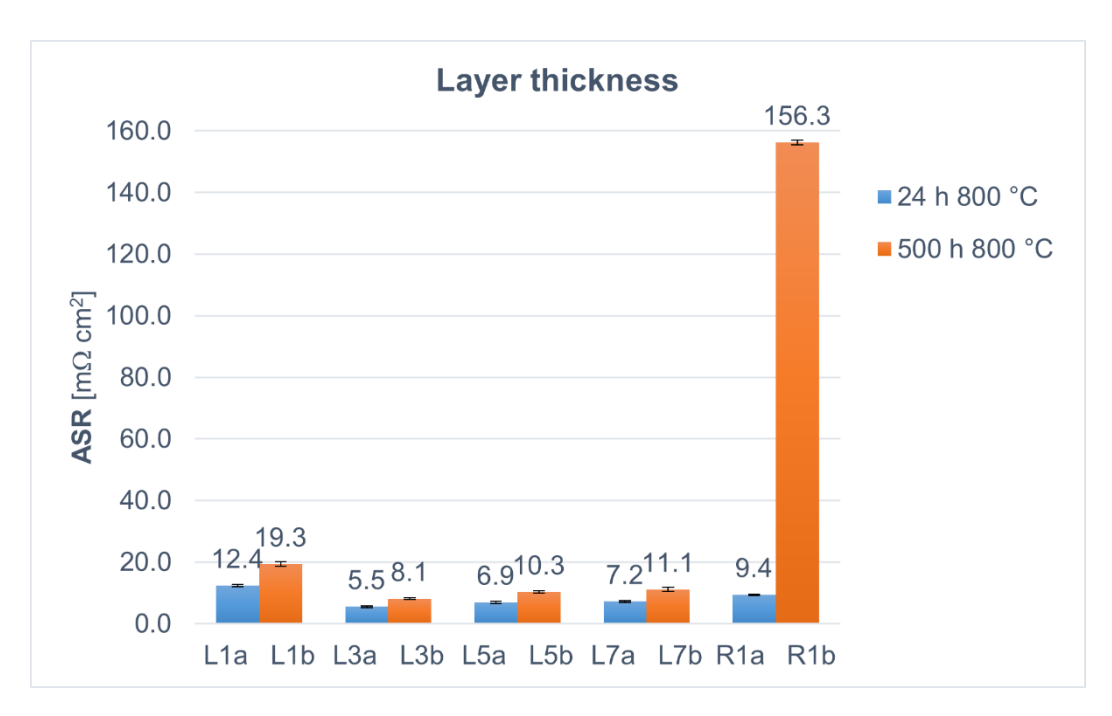


Figure 4: ASR values measured (a) after calcination and (b) after thermal treatment for 500 h at 800 °C. Samples coated with one (L1), three (L3), five (L5), and seven (L7) layers and bare Crofer 22 H (R1) were tested.

According to Figure 4, the lowest ASR values were measured for samples with three layers of MCF, which correlates with a layer thickness of about 9 μm. Applying only one layer of MCF resulted in surprisingly high ASR values. SEM overview images of the surface (not shown) revealed a crack-free microstructure. However, they also revealed several pores with diameters in the range of 1–10 μm. These defects did not occur for samples with multi-layer structure. The inferior coating quality and hence ASR performance could be traced back to an insufficient WPS spraying pattern of thin MCF single layers. In comparison to L3a/L3b, ASR values were slightly increased for L5a/L5b and L7a/L7b with five and seven layers of MCF, respectively. Initially, the ASR of uncoated Crofer 22H started in a similar range as for the coated samples (R1a). Nevertheless, a drastic increase of an order of magnitude was measured after thermal aging for 500 h (R1b). This was due to the formation of a thick, high-resistive chromia scale that is well known for chromium steels.

Considering the previously discussed risk of coating defect formation for WPS coatings with increased layer thickness, topologic profiles were conducted via white light interferometry (Figure 5). For samples with one and three MCF layers, rather smooth surfaces with pinholes of shallow depth were detected. In contrast, an increased surface roughness and larger pinhole defects were observed for five- and seven-layered samples. Even though ASR values were only slightly higher for L5 and L7, this effect may become more relevant under real conditions. The reason is that platinum contacting paste for ASR testing purposes is assumed to level out uneven surfaces. In contrast to real conditions, interconnect surfaces are directly contacted to another ceramic layer.

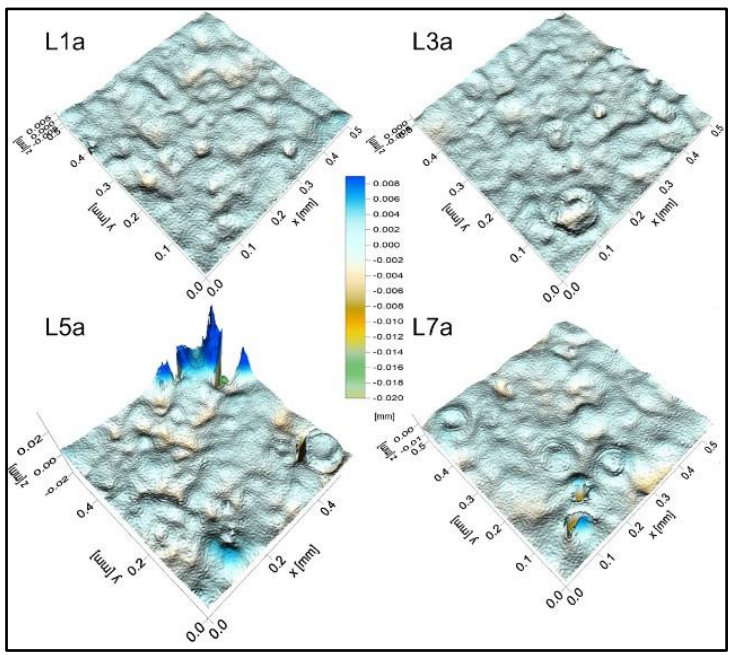


Figure 5: Topologic profiles of Crofer 22 H coated with one (L1a), three (L3a), five (L5a), and seven (L7a) layers of MCF.

In conclusion, the different performances observed were not related to the coating thickness itself, but rather to the associated changes in surface morphology and microstructure. The application of three layers of MCF represented the golden mean between performance and efficiency. There was no obvious advantage in crossing a threshold of 10 μ m in coating thickness for a WPS-based application of MCF.

3.4 Post-treatment

Spinel coatings applied by slurry-based techniques and sintered directly in air usually result in a microstructure with open porosity. This is accompanied by a rapid increase in area-specific contact resistance due to the formation of poorly conducting chromium oxides at the unprotected interface interconnect/protection layer. Although a densification of (Mn,Co)-based spinel coatings under stack conditions (700–850 °C, air) is desirable, reactive sintering remains the most effective way to achieve an adequate coating density and decrease interconnect degradation and thus ensure long-term stack stability. This section will focus on the impact of post-treatment

parameters on the protective layer microstructure and the correlation with the respective contact resistance value. Prior to thermal treatment, three layers of MCF were applied to all Crofer 22 H samples in an identical procedure utilizing a coating speed of 230mm/s. After reduction of the MCF to MnO and Co in Ar/H $_2$ 3 % at elevated temperatures, the reduced layer was re-oxidized in air. Various post-treatment parameter combinations, namely reduction temperature (T_{RED}), reduction duration (d_{RED}), oxidation temperature (T_{OX}), and oxidation duration (d_{OX}), were tested (Table 1). Thermal treatment was conducted with temperatures ranging between 800 °C to 1000 °C and holding times ranging between 2 h and 100 h. The temperatures and times were selected on the basis of i) retaining the metals' physical parameters (i.e. avoid creeping or fast oxidation); ii) actual stack start-up procedures; and iii) goals for the protective layer like densification, adhesion, or cracking.

Table 1: Thermal processing parameters for samples S1–S6 and results for porosity, interlayer thickness, and ASR.

	T _{RED} [°C]	d _{RED} [h]	T _{ox} [°C]	d _{ox} [h]	Porosity [%]	I(MIN) [µm]	I(MAX) [µm]	ASR [mΩ cm²]
S1	1000	2	1000	10	8.4(1)	0.5	1.1	5.6(1)
S2	1000	2	900	48	8.9(3)	1.1	1.3	8.0(3)
S3	1000	2	800	48	14.6(5)	1.1	1.5	11.9(4)
S4	900	12	900	12	8.5(1)	1.3	1.7	19.4(1)
S5	900	12	850	100	8.9(2)	1.0	1.7	15.4(6)
S6	850	24	850	100	13.3(2)	1.3	2.3	24.9(6)

According to the microstructure and calculated porosity of the selected sections, the results can be divided into two groups: low porosity below 9 % (S1, S2, S4, S5) and high porosity above 13 % (S3, S6). Cross-sections of the layers and the region evaluated for porosity determination are shown in Figure 6. Considering only porosity and time-efficiency, the sintering programs for S1 and S4 were the favored parameter settings. ASR values determined for coated samples S1-S6 did, however, reveal a slightly different picture (see Figure 6). With T_{RED} = 1000 °C, ASR values for S1-S3 were inversely proportional to the oxidation temperature. This trend was consistent with a decreasing sintering activity and thus increasing porosity of the protective layer from S1 to S3. The results for S4, S5, and S6 were less consistent. The highest ASR was measured for S6 despite the comparable porosity to S3. The ASR of S5 was $5 \text{ m}\Omega \text{ cm}^2$ lower on average with an almost identical porosity compared to S4. With Tox 50 °C higher for S4, the opposite result was expected. A possible explanation for this deviation could be the increased sintering activity due to the increased holding time of 100 h. The negative impact on the ASR by lowering the TRED could not be counterbalanced by increasing the holding time (S4 vs. S2). A high reduction temperature of 1000 °C with low holding times was therefore crucial to obtain the best results. This can be explained by the enhanced reaction rate from MCF to its reduced form MnO/Co/Fe, which facilitates better sintering in the downstream oxidation step. High oxidation temperatures benefit lower ASR values as well. However, the impact of a decreased Tox is lower and viable ASR values were still achievable. This facilitates densification of the protective layer during stack formation (850 °C, 100 h) and reduces the energy and time consumption of thermal processing significantly.

Overall, the degree of porosity alone could not provide sufficient assessment of the sintering parameters. As previously discussed, a negative influence on ASR was expected in dependence on the $Cr_2O_3/MnCr_2O_4$ interlayer thickness. Therefore, minimum (I(MIN)) and maximum interlayer thickness (I(MAX)) values of this scale were measured for each SEM cross section S1–S6. Including these values and the sum of both (labeled as I(TOTAL)) made the ASR measurement data more comprehensible (**Fehler! Verweisquelle konnte nicht gefunden werden.**). The higher the interlayer scale thickness, the higher the ASR, and thus the less favored the parameter set for sintering. This agrees with previous studies, and corresponds to the reduced electrical conductivity of Cr_2O_3 and $MnCr_2O_4$ compared to MCF. High reduction temperatures were needed to promote proper and fast densification during oxidation, reduce thickness of the interlayer scale during thermal treatment, and hence reduce the contact resistance.

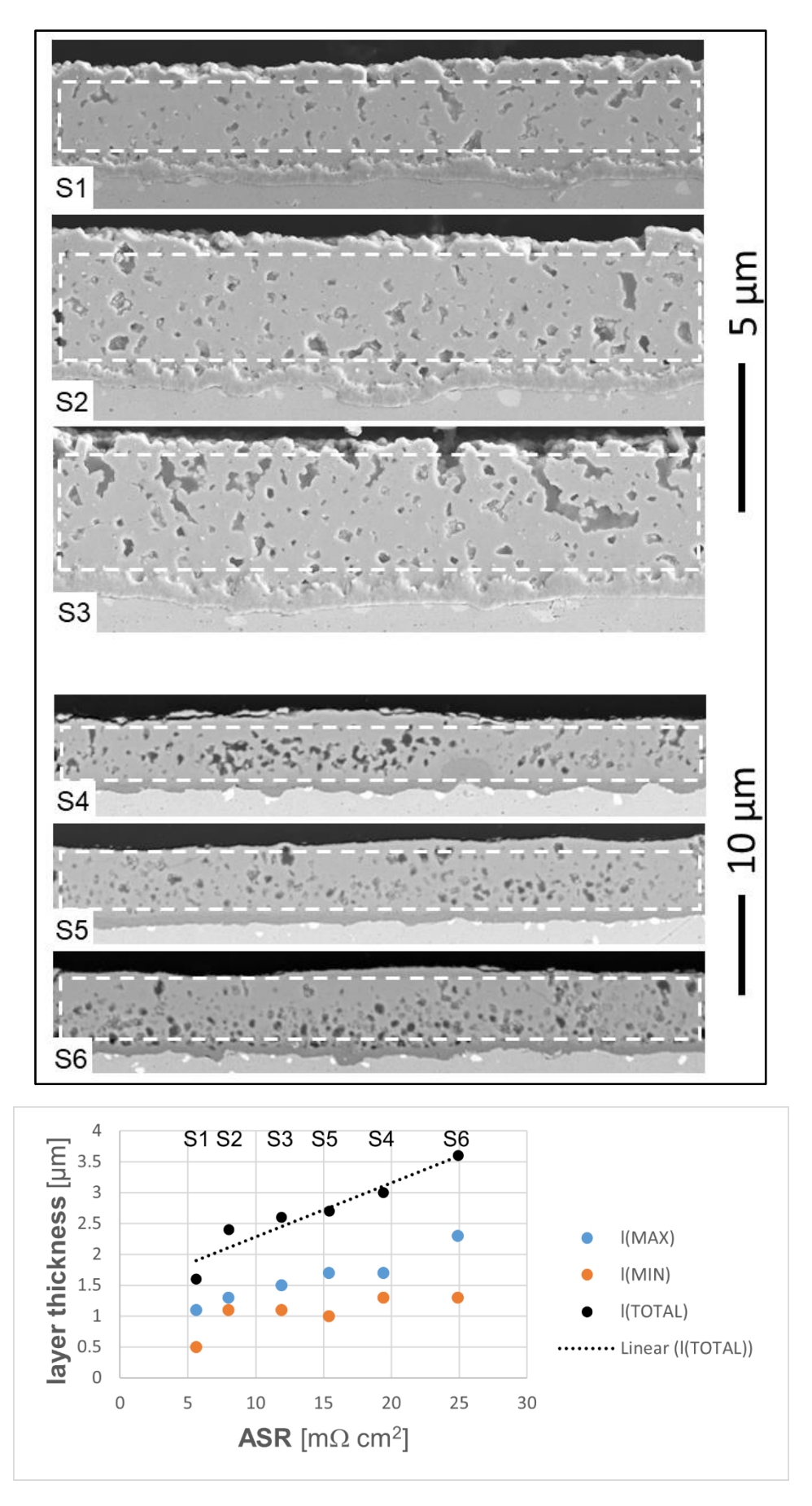


Figure 6: S1-S6: SEM cross sectional images of MCF-coated Crofer 22 H samples, which underwent different thermal post-processing. The segments for porosity determination are positioned over the SEM images as an overlay with 20 % transparency and dashed white lines (Please note that the magnifications shown for samples

3.5 Mid-term stability

An ASR of 20 m Ω cm² is often regarded as a threshold for quality evaluation in midterm and long-term thermal testing scenarios for SOC interconnect coatings [8,31–34]. Although this criterion is met for all samples L1b, L3b, L5b, and L7b after thermal treatment for 500 h at 800 °C, considerable performance differences were observed (cf. Figure 4). To confirm the improved performance of sample L3, a time-dependent study over 1000 h was conducted and compared to an uncoated Crofer 22 H substrate (Figure 7). Starting with an initial ASR of 6.5 m Ω cm², only a slight increase to 7.8 m Ω cm² was measured after 1000 h operation. The resulting value after 500 h thermal treatment (7.4 m Ω cm²) agreed well with the ex situ sample L3b (8.4 m Ω cm²). Surprisingly, the ASR increase in uncoated Crofer 22 H was much slower (500 h at 800 °C: 19.6 m Ω cm²; 1000 h at 800 °C: 25.2 m Ω cm²) compared to sample R1, which was thermally aged prior to testing (500 h at 800 °C: 156.3 m Ω cm²). A reasonable explanation for this finding is a passivation of the steel surface by the Pt paste, which was applied prior to the heat treatment. In the case of samples treated in an external furnace, the surface is exposed to air and more prone to chromia scale formation. Consequently, further uncoated interconnect substrates were thermally treated for 20 h, 100 h, and 400 h and tested. The resulting ASR amounted for 9.0 m Ω cm², 49.9 m Ω cm², and 96.2 m Ω cm², respectively. These results support the thesis of an enhanced oxidation resistance by platinum contacting paste. Due to similar ASR values measured for ex situ and in situ sample L3, an influence of platinum paste on the measurement of coated samples could be ruled out.

Overall, ASR values in the range of 5–10 m Ω cm² after 500 h or 1000 h, respectively, can be considered competitive results. Bianco et al. [33] compared WPS, APS, and PVD coatings of different materials on Crofer 22 H concluding best coating solution was a Fe-doped MnCo₂O₄ deposited by PVD resulting in 5mohm cm² at 1000 h of testing. According to the reported ASR values after 1000 h at 700 °C, coatings derived by two different WPS processes led to considerably poorer performances (20 m Ω cm² and 38 m Ω cm², respectively) The authors attributed this to an irregular shape of the interlayer and the high porosity of the WPS-derived coatings. Molin et al. [30] used electrophoretic deposition, thermal co-evaporation and RF magnetron sputtering. Despite showing high porosity with just a dense layer at the interface electrophoretic deposition showed lowest ASR with 22mohm cm² after 5000 h of oxidation and a three times lower degradation rate.

Figure 8 shows SEM and EDS measurements of MCF WPS-coated Crofer 22 H with processing parameters analogous to S1 and L3 followed by thermal aging at 800 °C for 1000 h in air. In contrast to the previous planar samples, the Crofer 22 H substrate was cut out of a real component interconnect with channel-type structure. The SEM overview image of the coated surface proved good adherence of the MCF layer over the whole component surface, even in the critical edge region. No cracks or delamination could be observed. Several pores enlarged during the mid-term thermal

treatment. EDS elemental maps were conducted for the relevant elements, namely manganese, cobalt, iron, and chromium. No increased Cr migration could be observed, neither at the edges nor in areas with enlarged pores. Furthermore, the enlarged area of the EDS elemental mapping revealed the presence of what is assumed to be $Mn_xCr_yO_4$ (greyish) and Cr_2O_3 (deep blue) at the interface interconnect/protective layer. The EDS map suggests that $Mn_xCr_yO_4$ contains some Co. Cr_2O_3 might react with MCF and form $(Mn_rCr_rCo)_3O_4$ where the higher Cr content probably decreases electrical conductivity.

We already tested a stack with two layers being coated with an MCF protective layer applied by non-optimized WPS but with redox treatment and two layers non post-treated for comparison. The stack was tested for almost 3500 h. Unfortunately, both inner layers, one with and one without pre-treatment, showed contacting issues leading to data with insufficient quality for evaluation. But to visualize a first behavior comparison of treated and untreated interconnects we put a Figure of this stack test in an added Supplementary (Figure S1). At the moment another stack with MCF protective coatings applied by WPS is under assembly and will be tested in the near future to evaluate long-term performance of the optimized WPS MCF coatings.

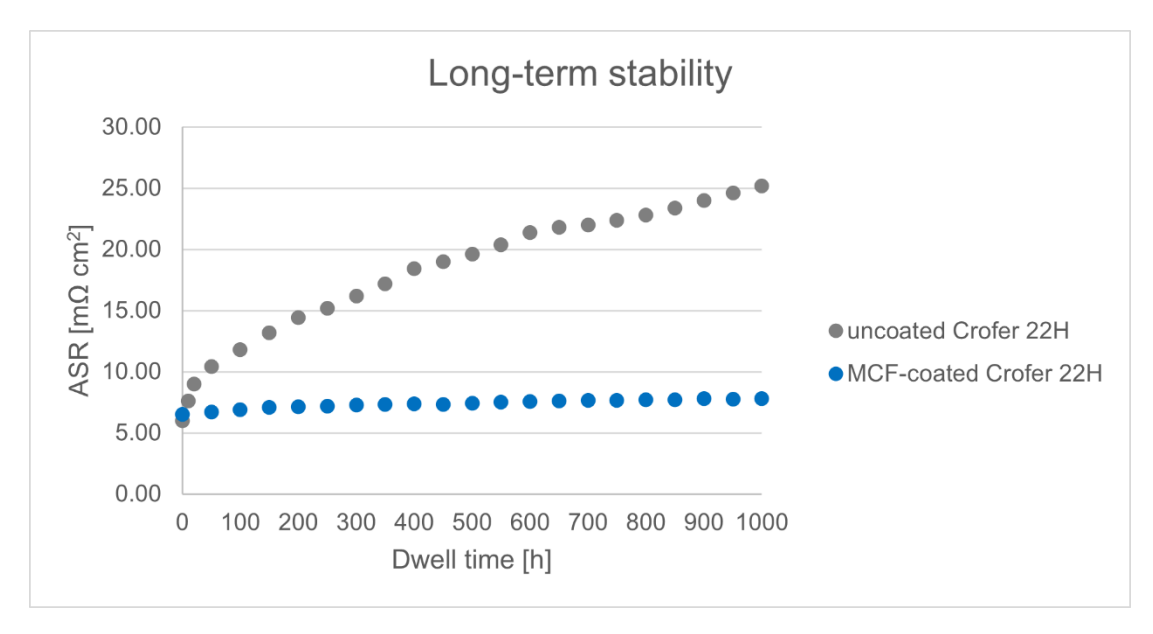


Figure 7: Time-dependent ASR measurement over 1000 h at 800 °C showing the contrasting ASR development for MCF-coated and uncoated Crofer 22 H.

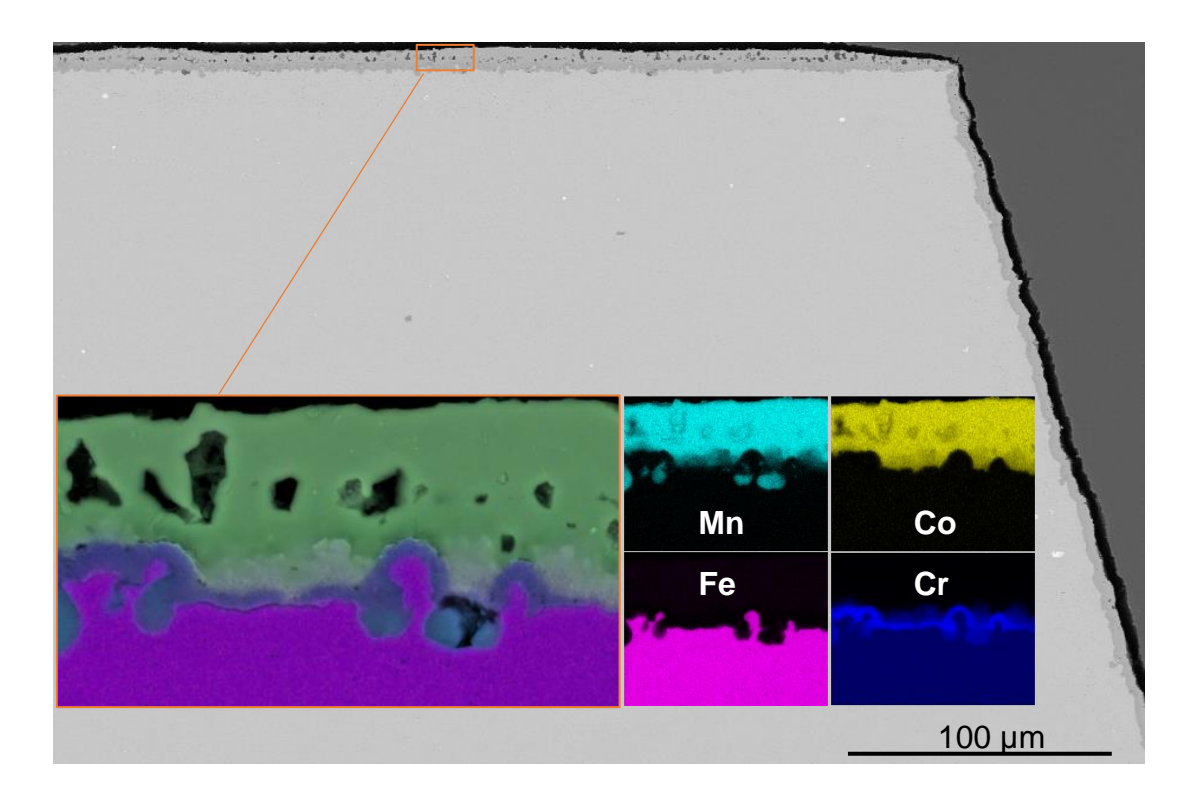


Figure 8: SEM cross sectional overview of channel-type Crofer 22 H coated with MCF after thermal treatment for 1000 h at 800 °C. The enlarged segment shows the EDS combined elemental map for Mn, Co, Fe, and Cr. The separated elemental maps demonstrate good Cr retention of the protective coating in mid-term operation.

4. Conclusion

In the past, WPS has often been considered inferior to other coating techniques due to their characteristic porous microstructure and comparably high ASR values. The present study highlighted the advantages of combining the well-known interconnect coating material Mn_{1.0}Co_{1.9}Fe_{0.1}O₄ with wet powder spraying, a highly efficient and scalable slurry coating technique. For the first time, a detailed study on the complex interplay between WPS and post-processing parameters and between interlayer microstructure and contact resistance was presented here. This study identified the most suitable parameter set, leading to competitive ASR values, significantly lower than previously published results for WPS-derived interconnect coatings.

The production of protective layers with a thickness above 20 μ m was rather challenging due to the formation of cracks and pinhole defects. However, a coating thickness in the range of 10 μ m derived by the application of three MCF layers and thermal treatment at 1000 °C was found to be most effective. According to microstructural analysis, protective layers remained mechanically and chemically stable with improved Cr retention and contact resistance in mid-term operation for 1000 h at 800 °C for planar as well as channel-type interconnect steel substrates. Time-dependent measurements over 1000 h confirmed the improved degradation resistance of MCF-coated Crofer 22 H with an ASR increase rate of only 0.13 m Ω cm²/100 h. (Limited improvement was achieved for single-layered coatings and thermal treatment at temperatures below 900 °C.)

Overall, wet powder spraying has shown great potential as a highly efficient, scalable, and economically viable technique for the application of gas-tight ceramic protective layers in the micrometer range. A batch process with processing times of a few seconds is equally as conceivable as a continuous process involving roll-to-roll coating.

Acknowledgements

Financial support from the German Federal Ministry of Education and Research (BMBF) is gratefully acknowledged. The translation group at the Forschungszentrum Jülich is acknowledged for their English grammar checking. Ute de Haart from IEK-9 of Forschungszentrum Jülich is gratefully acknowledged for performing the stack test.

Author contributions

MW: Writing original draft, conceptualization, data curation, investigation; AS: Review & editing. KW: Investigation and data curation, review and editing; DS: Investigation and data curation, review and editing; NHM: Funding acquisition, supervision, writing partly original draft and review & editing.

Funding

The work was funded by the German Ministry of Education and Research (BMBF) under contract No. 03SF0621A.

References

- [1] W.J. Quadakkers, J. Piron-Abellan, V. Shemet, L. Singheiser, Metallic interconnectors for solid oxide fuel cells a review, Materials at High Temperatures. 20 (2003) 115–127. https://doi.org/10.1179/mht.2003.015.
- [2] Z. Yang, Recent advances in metallic interconnects for solid oxide fuel cells, International Materials Reviews. 53 (2008) 39–54. https://doi.org/10.1179/174328007X212526.
- [3] J.G. Grolig, J. Froitzheim, J.-E. Svensson, Coated stainless steel 441 as interconnect material for solid oxide fuel cells: Oxidation performance and chromium evaporation, Journal of Power Sources. 248 (2014) 1007–1013. https://doi.org/10.1016/j.jpowsour.2013.08.089.
- [4] N. Manjunath, K. Santhy, B. Rajasekaran, Thermal expansion of Crofer 22 APU steel used for SOFC interconnect using in-situ high temperature X-ray diffraction, Materials Today: Proceedings. (2023). https://doi.org/10.1016/j.matpr.2023.03.113.
- [5] K. Hilpert, D. Das, M. Miller, D.H. Peck, R. Weiß, Chromium Vapor Species over Solid Oxide Fuel Cell Interconnect Materials and Their Potential for Degradation Processes, J. Electrochem. Soc. 143 (1996) 3642. https://doi.org/10.1149/1.1837264.
- [6] M. Stanislowski, J. Froitzheim, L. Niewolak, W.J. Quadakkers, K. Hilpert, T. Markus, L. Singheiser, Reduction of chromium vaporization from SOFC

- interconnectors by highly effective coatings, Journal of Power Sources. 164 (2007) 578–589. https://doi.org/10.1016/j.jpowsour.2006.08.013.
- [7] B. Talic, V. Venkatachalam, P.V. Hendriksen, R. Kiebach, Comparison of MnCo2O4 coated Crofer 22 H, 441, 430 as interconnects for intermediatetemperature solid oxide fuel cell stacks, Journal of Alloys and Compounds. 821 (2020) 153229. https://doi.org/10.1016/j.jallcom.2019.153229.
- [8] J.H. Zhu, D.A. Chesson, Y.T. Yu, Review—(Mn,Co)3O4-Based Spinels for SOFC Interconnect Coating Application, J. Electrochem. Soc. 168 (2021) 114519. https://doi.org/10.1149/1945-7111/ac3a29.
- [9] T. Horita, LaCrO3-Based Perovskite for SOFC Interconnects, in: T. Ishihara (Ed.), Perovskite Oxide for Solid Oxide Fuel Cells, Springer US, Boston, MA, 2009: pp. 285–296. https://doi.org/10.1007/978-0-387-77708-5_15.
- [10] N. Sakai, H. Yokokawa, T. Horita, K. Yamaji, Lanthanum Chromite-Based Interconnects as Key Materials for SOFC Stack Development, International Journal of Applied Ceramic Technology. 1 (2004) 23–30. https://doi.org/10.1111/j.1744-7402.2004.tb00151.x.
- [11] J.H. Zhu, Y. Zhang, A. Basu, Z.G. Lu, M. Paranthaman, D.F. Lee, E.A. Payzant, LaCrO3-based coatings on ferritic stainless steel for solid oxide fuel cell interconnect applications, Surface and Coatings Technology. 177–178 (2004) 65– 72. https://doi.org/10.1016/j.surfcoat.2003.05.003.
- [12] T. Brylewski, K. Przybylski, Perovskite and Spinel Functional Coatings for SOFC Metallic Interconnects, Materials Science Forum. 595–598 (2008) 813–822. https://doi.org/10.4028/www.scientific.net/MSF.595-598.813.
- [13] B. Talic, S. Molin, K. Wiik, P.V. Hendriksen, H.L. Lein, Comparison of iron and copper doped manganese cobalt spinel oxides as protective coatings for solid oxide fuel cell interconnects, Journal of Power Sources. 372 (2017) 145–156. https://doi.org/10.1016/j.jpowsour.2017.10.060.
- [14] N. Hosseini, M.H. Abbasi, F. Karimzadeh, G.M. Choi, Development of Cu1.3Mn1.7O4 spinel coating on ferritic stainless steel for solid oxide fuel cell interconnects, Journal of Power Sources. 273 (2015) 1073–1083. https://doi.org/10.1016/j.jpowsour.2014.10.017.
- [15] Z. Sun, S. Gopalan, U.B. Pal, S.N. Basu, Cu1.3Mn1.7O4 spinel coatings deposited by electrophoretic deposition on Crofer 22 APU substrates for solid oxide fuel cell applications, Surface and Coatings Technology. 323 (2017) 49–57. https://doi.org/10.1016/j.surfcoat.2016.09.028.
- [16] N. Shaigan, W. Qu, D.G. Ivey, W. Chen, A review of recent progress in coatings, surface modifications and alloy developments for solid oxide fuel cell ferritic stainless steel interconnects, Journal of Power Sources. 195 (2010) 1529– 1542. https://doi.org/10.1016/j.jpowsour.2009.09.069.
- [17] E. Dogdibegovic, S. Ibanez, A. Wallace, D. Kopechek, G. Arkenberg, S. Swartz, J.M. Funk, M. Reisert, M.A. Rahman, A. Aphale, P. Singh, H. Ding, W. Tang, M.V. Glazoff, D. Ding, T.L. Skafte, M.C. Tucker, Performance of stainless steel interconnects with (Mn,Co)3O4-Based coating for solid oxide electrolysis, International Journal of Hydrogen Energy. 47 (2022) 24279–24286. https://doi.org/10.1016/j.ijhydene.2022.05.206.
- [18] F. Smeacetto, A. De Miranda, S. Cabanas Polo, S. Molin, D. Boccaccini, M. Salvo, A.R. Boccaccini, Electrophoretic deposition of Mn1.5Co1.5O4 on metallic interconnect and interaction with glass-ceramic sealant for solid oxide fuel cells application, Journal of Power Sources. 280 (2015) 379–386. https://doi.org/10.1016/j.jpowsour.2015.01.120.

- [19] M.J. Reddy, J.-E. Svensson, J. Froitzheim, Reevaluating the Cr Evaporation Characteristics of Ce/Co Coatings for Interconnect Applications, ECS Trans. 103 (2021) 1899. https://doi.org/10.1149/10301.1899ecst.
- [20] N. Grünwald, P. Lhuissier, L. Salvo, J. Villanova, N.H. Menzler, O. Guillon, C.L. Martin, R. Vaßen, In situ investigation of atmospheric plasma-sprayed Mn—Co–Fe–O by synchrotron X-ray nano-tomography, J Mater Sci. 55 (2020) 12725–12736. https://doi.org/10.1007/s10853-020-04916-9.
- [21] A. Kruk, M. Stygar, T. Brylewski, Mn–Co spinel protective–conductive coating on AL453 ferritic stainless steel for IT-SOFC interconnect applications, J Solid State Electrochem. 17 (2013) 993–1003. https://doi.org/10.1007/s10008-012-1952-8.
- [22] A. Ruder, H.P. Buchkremer, H. Jansen, W. Malléner, D. Stöver, Wet powder spraying—a process for the production of coatings, Surface and Coatings Technology. 53 (1992) 71–74. https://doi.org/10.1016/0257-8972(92)90105-J.
- [23] L. Zhao, M. Bram, H.P. Buchkremer, D. Stöver, Z. Li, Preparation of TiO2 composite microfiltration membranes by the wet powder spraying method, Journal of Membrane Science. 244 (2004) 107–115. https://doi.org/10.1016/j.memsci.2004.07.010.
- [24] VDM-Metals, Crofer22H Data Sheet, (2010).
- [25] N. Grünwald, Y.J. Sohn, X. Yin, N.H. Menzler, O. Guillon, R. Vaßen, Microstructure and phase evolution of atmospheric plasma sprayed Mn-Co-Fe oxide protection layers for solid oxide fuel cells, Journal of the European Ceramic Society. 39 (2019) 449–460. https://doi.org/10.1016/j.jeurceramsoc.2018.08.027.
- [26] Z. Yang, G. Xia, S.P. Simner, J.W. Stevenson, Thermal Growth and Performance of Manganese Cobaltite Spinel Protection Layers on Ferritic Stainless Steel SOFC Interconnects, J. Electrochem. Soc. 152 (2005) A1896. https://doi.org/10.1149/1.1990462.
- [27] Y. Jin, J. Sheng, G. Hao, M. Guo, W. Hao, Z. Yang, X. Xiong, S. Peng, Highly dense (Mn,Co)3O4 spinel protective coating derived from Mn–Co metal precursors for SOFC interconnect applications, International Journal of Hydrogen Energy. 47 (2022) 13960–13968. https://doi.org/10.1016/j.ijhydene.2022.02.129.
- [28] M.J. Reddy, B. Kamecki, B. Talic, E. Zanchi, F. Smeacetto, J.S. Hardy, J.P. Choi, Ł. Mazur, R. Vaßen, S.N. Basu, T. Brylewski, J.-E. Svensson, J. Froitzheim, Experimental review of the performances of protective coatings for interconnects in solid oxide fuel cells, Journal of Power Sources. 568 (2023) 232831. https://doi.org/10.1016/j.jpowsour.2023.232831.
- [29] P. Huczkowski, N. Christiansen, V. Shemet, L. Niewolak, J. Piron-Abellan, L. Singheiser, W.J. Quadakkers, Growth Mechanisms and Electrical Conductivity of Oxide Scales on Ferritic Steels Proposed as Interconnect Materials for SOFC's, Fuel Cells. 6 (2006) 93–99. https://doi.org/10.1002/fuce.200500110.
- [30] S. Molin, A.G. Sabato, M. Bindi, P. Leone, G. Cempura, M. Salvo, S. Cabanas Polo, A.R. Boccaccini, F. Smeacetto, Microstructural and electrical characterization of Mn-Co spinel protective coatings for solid oxide cell interconnects, Journal of the European Ceramic Society. 37 (2017) 4781–4791. https://doi.org/10.1016/j.jeurceramsoc.2017.07.011.
- [31] M.A. Hassan, O.B. Mamat, M. Mehdi, Review: Influence of alloy addition and spinel coatings on Cr-based metallic interconnects of solid oxide fuel cells, International Journal of Hydrogen Energy. 45 (2020) 25191–25209. https://doi.org/10.1016/j.ijhydene.2020.06.234.
- [32] P. Piccardo, P. Gannon, S. Chevalier, M. Viviani, A. Barbucci, G. Caboche, R. Amendola, S. Fontana, ASR evaluation of different kinds of coatings on a ferritic

- stainless steel as SOFC interconnects, Surface and Coatings Technology. 202 (2007) 1221–1225. https://doi.org/10.1016/j.surfcoat.2007.07.096.
- [33] M. Bianco, J. Tallgren, J.-E. Hong, S. Yang, O. Himanen, J. Mikkola, J. Van herle, R. Steinberger-Wilckens, Ex-situ experimental benchmarking of solid oxide fuel cell metal interconnects, Journal of Power Sources. 437 (2019) 226900. https://doi.org/10.1016/j.jpowsour.2019.226900.
- [34] M. Bianco, P. Caliandro, S. Diethelm, S. Yang, A. Dellai, J. Van herle, R. Steinberger-Wilckens, In-situ experimental benchmarking of solid oxide fuel cell metal interconnect solutions, Journal of Power Sources. 461 (2020) 228163. https://doi.org/10.1016/j.jpowsour.2020.228163.